Dark matter detectors as a novel probe for light new physics

Anirban Majumdar,[1,*] D. K. Papoulias,[2,†] and Rahul Srivastava[1,‡]
[1]*Department of Physics, Indian Institute of Science Education and Research-Bhopal, Bhopal Bypass Road, Bhauri, Bhopal 462066, India*
[2]*Division of Theoretical Physics, University of Ioannina, GR 45110 Ioannina, Greece*

(Received 14 December 2021; accepted 23 June 2022; published 6 July 2022)

We explore the prospect of constraining light mediators at the next generation direct detection dark matter detectors through coherent elastic neutrino-nucleus scattering (CEνNS) and elastic neutrino-electron scattering (EνES) measurements. Taking into account various details like the quenching factor corrections, atomic binding effects, realistic backgrounds, detection efficiency, energy resolution, etc., we consider two representative scenarios regarding detector specifications. For both scenarios, we obtain the model-independent projected sensitivities for all possible Lorentz-invariant interactions, namely, scalar (S), pseudoscalar (P), vector (V), axial vector (A), and tensor (T). For the case of vector interactions, we also focus on two concrete examples: the well-known $U(1)_{B-L}$ and $U(1)_{L_\mu - L_\tau}$ gauge symmetries. For all interaction channels $X = \{S, P, V, A, T\}$, our results imply that the upcoming dark matter detectors have the potential to place competitive constraints, improved by about 1 order of magnitude compared to existing ones from dedicated CEνNS experiments, XENON1T, beam dump experiments, and collider probes.

DOI: 10.1103/PhysRevD.106.013001

I. INTRODUCTION

Although the Standard Model (SM) provides a rather successful description of electroweak and strong interactions in nature, there is a list of shortcomings that points to the need of new physics beyond the Standard Model (BSM). Usually, it is assumed that the scale of such new physics is larger than the electroweak symmetry breaking scale and the new BSM particles are heavy. For example, the existence of new neutral Z' gauge bosons under an extra gauge symmetry is a common feature of many theories beyond the SM [1]. Extensive phenomenological studies at colliders [2] have been performed, taking the Z' bosons to be heavier than electroweak scale.

However, there exist various motivated BSM extensions where the new physics is desirable to be at the low scale. Light new physics, for example, can account for the explanation of existing anomalies, such as the longstanding anomalous magnetic moment of muons [3–5]. Moreover, concerning the dark sector, several dark matter models require the presence of light mediators to account for dark matter self-interaction [6,7] and/or the recent XENON1T anomaly [8–10]. Finally, the Peccei-Quinn solutions of the strong CP problem also imply the presence of a light Nambu-Goldstone boson called an axion [11–13], while neutrino mass models involving dynamical lepton number breaking often lead to a light pseudoscalar boson called Majoron (Majorana neutrinos) or Diracon (Dirac neutrinos) [14,15].

While the implications of light vector and scalar mediators to the expected signal rates had already been explored at direct detection dark matter experiments [16,17], after the recent observation of coherent elastic neutrino-nucleus scattering (CEνNS) by the COHERENT experiment [18–20] there has been an intense interest for novel mediator investigations [21–28]. In addition to COHERENT, data-driven constraints also exist from upper limits on CEνNS, placed by the recent CONNIE [29] and CONUS [30] measurements. Phenomenological studies focusing on various $U'(1)$ realizations, such as the $L_\mu - L_\tau$ and $B - L$ gauge symmetries have been explored using solar neutrinos [31–33], as well as using supernova neutrinos taking also into account corrections from medium effects [34]. It is interesting to note that the latter can induce a reduction of the cross section due to Pauli blocking and therefore lead to less severe constraints. Very recently, the expected modification to the neutrino floor has been illustrated in the presence of vector and scalar mediators [35], while the complementarity of CEνNS and direct

*anirban19@iiserb.ac.in
†d.papoulias@uoi.gr
‡rahul@iiserb.ac.in

detection dark matter experiments was emphasized through a data-driven analysis of the neutrino floor.

In addition to scalar and vector mediator scenarios, it is possible to explore further Lorentz-invariant structures, such as scalar (S), pseudoscalar (P), vector (V), axial vector (A), or tensor (T) interactions in a model-independent way through neutrino generalized interactions (NGIs). Assuming heavy mediators, NGIs have been explored in Ref. [36] using CEνNS data from COHERENT and in Ref. [37] through elastic neutrino-electron scattering (EνES) by analyzing the Borexino data. Reference [38] performed a global NGI analysis in the light data from EνES experiments, neutrino deep inelastic scattering, and single-photon detection from electron-positron collisions, while Ref. [39] pointed out the possibility of probing the Dirac or Majorana neutrino nature through NGIs. Tensorial exotic interactions have been explored in Ref. [40] using the TEXONO data, as well as in Ref. [41] where their connection to neutrino transition magnetic moments was emphasized. Finally, constraints in the tensor parameter space were extracted from the analysis of COHERENT data [42] and more recently by the CONUS Collaboration [30].

The next generation direct detection dark matter experiments with multiton mass scale and sub-keV capabilities are expected to become sensitive to astrophysical neutrinos. Indeed, the XENON1T Collaboration has already reported first results in its effort to identify a potential CEνNS population—induced by ^{8}B neutrinos of the solar flux—in the background data [43]. Motivated by the upcoming large scale next generation direct detection dark matter experiments, such as XENONnT [44], in this work we consider the possibility of exploring neutrino backgrounds using nuclear and electron recoils. In particular, we are interested to explore the prospects of constraining general neutrino interactions induced by novel mediators via CEνNS and EνES measurements at a future direct detection dark matter experiment. Unlike previous studies—especially for the cases of pseudoscalar, axial vector, and tensor interaction channels—we allow the exchanged mediator to be sufficiently light. Therefore, for all possible interaction channels, the dependence on the mediator mass has been considered explicitly in the cross sections. Our present results indicate that future dark matter detectors will offer competitive constraints in the mass-coupling parameter space, being also complementary to collider probes and DUNE.

The remainder of the paper has been organized as follows. In Sec. II, we provide the necessary formalism regarding CEνNS processes. We start with the discussion of CEνNS within the SM and then discuss the new physics contribution to it. In Sec. III, we discuss the case of EνES, again starting with the SM discussion and ending with the new physics contribution. Our main results are presented in Sec. IV, where we first discuss the model-independent constraints on various types of new physics scenarios. We then, as examples, take a few specific models with light mediators and further analyze our constraints, comparing and contrasting them with constraints obtained from other experimental probes. Our concluding remarks are summarized in Sec. V.

II. COHERENT ELASTIC NEUTRINO-NUCLEUS SCATTERING

In this section, we provide the basic formalism for the description of the various CEνNS interaction channels considered in the present work, within and beyond the SM. A model-independent analysis is performed by considering all possible Lorentz-invariant interaction channels in the low-energy regime. The latter can be conveniently classified in terms of the Lorentz and parity transformations of the mediator particle, i.e., whether the mediator transforms as S, P, V, A, or T. One further advantage of such parametrization is that interactions of any particle having a mixed transformation (e.g., SM Z^0 boson) can also be taken into account simply as a combination of S, P, V, A, T interactions.

A. CEνNS within the SM

Assuming SM interactions only, for low and intermediate neutrino energies ($E_\nu \ll M_{Z^0}$) CEνNS is accurately described in the context of an effective four-fermion Fermi interaction Lagrangian [45]

$$\mathcal{L}_{\rm SM} = -2\sqrt{2}G_F \sum_{\substack{f=u,d \\ \alpha=e,\mu,\tau}} g^{f,P}_{\alpha,\alpha}[\bar{\nu}_\alpha \gamma^\rho L \nu_\alpha][\bar{f}\gamma_\rho P f]. \quad (1)$$

Here, $P \equiv \{L, R\}$ stand for the chiral projection operators, $f \equiv \{u, d\}$ represents the first generation quark, and $g^{f,P}_{\alpha,\alpha}$ is the P-handed coupling of the quark f to the SM Z^0 boson. The latter are expressed in terms of the weak mixing angle ($\sin^2\theta_W = 0.2387$), as

$$g^{u,L}_{\alpha,\alpha} = \frac{1}{2} - \frac{2}{3}\sin^2\theta_W, \qquad g^{u,R}_{\alpha,\alpha} = -\frac{2}{3}\sin^2\theta_W,$$
$$g^{d,L}_{\alpha,\alpha} = -\frac{1}{2} + \frac{1}{3}\sin^2\theta_W, \qquad g^{d,R}_{\alpha,\alpha} = \frac{1}{3}\sin^2\theta_W. \quad (2)$$

At tree level,[1] the SM differential CEνNS cross section with respect to the nuclear recoil energy E_{nr} is given as [47]

$$\left[\frac{d\sigma}{dE_{nr}}\right]^{\nu N}_{\rm SM} = \frac{G_F^2 m_N}{\pi}(Q_V^{\rm SM})^2\left(1 - \frac{m_N E_{nr}}{2E_\nu^2}\right), \quad (3)$$

where G_F is the Fermi constant and m_N is the nuclear mass, while the SM vector weak charge $Q_V^{\rm SM}$ takes the form [48]

[1]Subdominant radiative corrections are discussed in Ref. [46].

$$Q_V^{\rm SM} = [g_p^V Z + g_n^V N] F_W(q^2). \tag{4}$$

Here, Z and N denote the number of protons and neutrons in the nucleus, while the corresponding vector couplings for protons (g_p^V) and neutrons (g_n^V) read [49]

$$\begin{aligned} g_p^V &= 2(g_{\alpha,\alpha}^{u,L} + g_{\alpha,\alpha}^{u,R}) + (g_{\alpha,\alpha}^{d,L} + g_{\alpha,\alpha}^{d,R}) = 1/2 - 2\sin^2\theta_W, \\ g_n^V &= (g_{\alpha,\alpha}^{u,L} + g_{\alpha,\alpha}^{u,R}) + 2(g_{\alpha,\alpha}^{d,L} + g_{\alpha,\alpha}^{d,R}) = -1/2. \end{aligned} \tag{5}$$

It is noteworthy that Eq. (3) is valid for sufficiently low momentum transfer in order to satisfy the coherency condition $q \leq 1/R_A$ [48], with R_A being the nuclear radius and $q^2 = 2m_N E_{nr}$ denoting the magnitude of three-momentum transfer. Moreover, to account for the finite nuclear spatial distribution, nuclear physics corrections are incorporated in Eq. (4) through the weak nuclear form factor $F_W(q^2)$. In our present study, we adopt the Helm parametrization, given as [50]

$$F_W(q^2) = \frac{3j_1(qR_0)}{qR_0} e^{[-\frac{1}{2}(qs)^2]}, \tag{6}$$

where $j_1(x)$ is the first-order spherical Bessel function, while the diffraction radius is given by $R_0^2 = \frac{5}{3}R^2 - 5s^2$, with the nuclear radius and surface thickness taken to be $R = 1.23A^{1/3}$ fm and $s = 0.9$ fm, respectively, with $A = N + Z$ being the atomic mass number.

B. CEνNS contribution from light novel mediators

NGIs constitute a useful model-independent probe that can accommodate several attractive BSM scenarios. By restricting ourselves to low-energy neutral-current interactions (below the electroweak symmetry breaking scale), in this work we consider general new physics interactions arising from the Lagrangian [36,51]

$$\mathcal{L}_{\rm NGI} = \frac{G_F}{\sqrt{2}} \sum_{\substack{X=S,P,V,A,T \\ f=u,d \\ \alpha=e,\mu,\tau}} C_{\alpha,\alpha}^{f,P} [\bar{\nu}_\alpha \Gamma^X L \nu_\alpha][\bar{f}\Gamma_X P f]. \tag{7}$$

Therefore, in what follows, all possible Lorentz-invariant structures are taken into account, i.e., $\Gamma_X = \{\mathbb{1}, i\gamma_5, \gamma_\mu, \gamma_\mu\gamma_5, \sigma_{\mu\nu}\}$ (with $\sigma_{\mu\nu} = \frac{i}{2}[\gamma_\mu, \gamma_\nu]$), corresponding to $X = \{S, P, V, A, T\}$ interactions, respectively. The dimensionless coefficients $C_{\alpha,\alpha}^{f,P}$ measure the relative strength of the new physics interaction X and are of the order of $(\sqrt{2}/G_F)(g_X^2/(q^2 + m_X^2))$ with m_X and g_X being the mass of the exchanged light mediator and the corresponding coupling, respectively. Throughout this work, we define the coupling $g_X = \sqrt{g_{\nu X} g_{fX}}$; $f = \{u, d\}$ for CEνNS and $f = e$ for EνES.

We proceed by relying on previous analyses [52,53] that, in the limit of vanishing momentum transfer, argued that the nucleonic matrix element of the quark current is proportional to that of the corresponding nucleon current $\langle N_f|\bar{q}\Gamma^X q|N_i\rangle \equiv \mathcal{F}^X(q)\langle N_f|\bar{N}\Gamma^X N|N_i\rangle$, where $\mathcal{F}^X(q)$ is the form factor calculated within the framework of nonperturbative low-energy QCD. The individual interactions and their contribution to the CEνNS differential cross section are listed in Table I. For the different interactions X, the relevant effective charges Q_X entering the respective cross sections are given by [16,40,53,54]

$$\begin{aligned} Q_s &= g_{\nu S}\left(Z\sum_q g_{qS}\frac{m_p}{m_q}f_q^p + N\sum_q g_{qS}\frac{m_n}{m_q}f_q^n\right)F_W(q^2), \\ Q_P &= g_{\nu P}\left(Z\sum_q g_{qP}\frac{m_p}{m_q}h_q^p + N\sum_q g_{qP}\frac{m_n}{m_q}h_q^n\right)F_W(q^2), \\ Q_V &= g_{\nu V}[(2g_{uV} + g_{dV})Z + (g_{uV} + 2g_{dV})N]F_W(q^2), \\ Q_A &= g_{\nu A}\left(ZS_p\sum_q g_{qA}\Delta_q^p + NS_n\sum_q g_{qA}\Delta_q^n\right)F_W(q^2), \\ Q_T &= g_{\nu T}\left(Z\sum_q g_{qT}\delta_q^p + N\sum_q g_{qT}\delta_q^n\right)F_W(q^2). \end{aligned} \tag{8}$$

In the latter expressions, the hadronic structure parameters for the scalar case (S) are $f_u^p = 0.0208$, $f_u^n = 0.0189$, $f_d^p = 0.0411$, and $f_d^n = 0.0451$ [55], for the pseudoscalar case (P) are $h_u^p = h_u^n = 1.65$ and $h_d^p = h_d^n = 0.375$ [56], and for the tensor case (T) are $\delta_u^p = \delta_d^n = 0.54$ and $\delta_d^p = \delta_u^n = -0.23$ [55]. Finally, for the case of axial vector (A) interactions, the hadronic parameters read $\Delta_u^p = \Delta_u^n = 0.842$ and $\Delta_d^p = \Delta_d^n = -0.427$ [57], while the spin expectation values (S_p and S_n) are nuclear model and isotope dependent. In the present study, we consider the following spin expectation values for protons (^{129}Xe: $S_p = 0.010$, ^{131}Xe: $S_p = -0.009$) and neutrons (^{129}Xe: $S_n = 0.329$, ^{131}Xe: $S_n = -0.272$), extracted from shell model nuclear structure calculations in Ref. [58].[2]

A few comments are in order. First, from Table I it becomes evident that for the case of S, P, A, T interactions there is an absence of interference with the SM CEνNS cross section, in contrast to the vector mediator case where the new physics contribution yields interference terms. For the sake of clarity we should stress that, in principle, the axial vector interaction adds incoherently to the SM CEνNS cross section, however, the SM axial contribution is significantly suppressed with respect to the vector one and therefore neglected (see Ref. [42]). Moreover, as discussed in Ref. [36], the existence of axial quark terms in the interaction Lagrangian (7) will lead to pseudoscalar-scalar neutrino-quark couplings, the study of which will be

[2]Even-even xenon isotopes with 0^+ ground state do not contribute to axial vector interactions because of angular momentum conservation.

TABLE I. Novel interactions $X = \{S, P, V, A, T\}$ and corresponding differential CEνNS cross sections considered in the present work. Because of interference, the V interaction is the only case that includes the SM contribution, while the S, P, A, T cases acquire contributions from new physics only, as shown in the cross sections (see the text for more details).

Mediator	$\mathcal{L}_X$	Cross section
Scalar	$[(g_{\nu S}\bar{\nu}_R\nu_L + \text{H.c.}) + \sum_{q=\{u,d\}} g_{qS}\bar{q}q]S + \frac{1}{2}m_S^2S^2$	$\frac{m_N^2E_{nr}Q_S^2}{4\pi E_\nu^2(q^2+m_S^2)^2}$
Pseudoscalar	$[(g_{\nu P}\bar{\nu}_R\gamma_5\nu_L + \text{H.c.}) - i\sum_{q=\{u,d\}} g_{qP}\bar{q}\gamma_5 q]P + \frac{1}{2}m_P^2P^2$	$\frac{m_N E_{nr}^2 Q_P^2}{8\pi E_\nu^2(q^2+m_P^2)^2}$
Vector	$[g_{\nu V}\bar{\nu}_L\gamma_\mu\nu_L + \sum_{q=\{u,d\}} g_{qV}\bar{q}\gamma_\mu q]V^\mu + \frac{1}{2}m_V^2V^\mu V_\mu$	$(1+\frac{Q_V}{\sqrt{2}G_F Q_V^{\rm SM}(q^2+m_V^2)})^2[\frac{d\sigma}{dE_{nr}}]_{\rm SM}^{\nu N}$
Axial vector	$[g_{\nu A}\bar{\nu}_L\gamma_\mu\gamma_5\nu_L - \sum_{q=\{u,d\}} g_{qA}\bar{q}\gamma_\mu\gamma_5 q]A^\mu + \frac{1}{2}m_A^2A^\mu A_\mu$	$\frac{m_N Q_A^2(2E_\nu^2+m_N E_{nr})}{4\pi E_\nu^2(q^2+m_A^2)^2}$
Tensor	$[g_{\nu T}\bar{\nu}_R\sigma_{\rho\delta}\nu_L - \sum_{q=\{u,d\}} g_{qT}\bar{q}\sigma_{\rho\delta}q]T^{\rho\delta} + \frac{1}{2}m_T^2T^{\rho\delta}T_{\rho\delta}$	$\frac{m_N Q_T^2(4E_\nu^2-m_N E_{nr})}{2\pi E_\nu^2(q^2+m_T^2)^2}$

relaxed as it goes well beyond the scope of our work. Finally, the P and A terms are spin-dependent and therefore suppressed with respect to S, V, T terms.[3] For the latter issue, we will rely on the assumption that the new physics interaction is controlled by the strength of the neutrino coupling.

Focusing on light vector mediators only, in this work we will consider three different models, determined by the charges of leptons Q'_ℓ and quarks Q'_q under the extra gauge symmetry $U(1)'$ [61]. First, we consider a generic model where the new vector mediator V couples universally to all SM fermions, such that $Q'_\ell = Q'_q = 1$, corresponding to an effective vector charge in Eq. (8) with $g_{qV} = g_{\nu V}$. Second, we focus on the U_{B-L} extension of the SM, in which the anomaly cancellation conditions $Q'_\ell = -1$ and $Q'_q = 1/3$ imply an effective vector charge with $g_{qV} = -g_{\nu V}/3$. Finally, we consider the gauged $U_{L_\mu - L_\tau}$ symmetry, where the new vector mediator boson couples directly only to muons and tauons with the absence of tree-level couplings to quarks. In this model, contributions to CEνNS are possible at the one-loop level, leading to an "effective" kinetic mixing between the new mediator and the SM photon [62], and the corresponding cross section reads [28,63]

$$\left[\frac{d\sigma}{dE_{nr}}\right]_{L_\mu-L_\tau}^{\nu N} = \left(1 \pm \frac{\alpha_{em} g_{\nu V} g_{qV} \log(\frac{m_\tau^2}{m_\mu^2}) Z F_W(q^2)}{3\sqrt{2}\pi G_F Q_V^{\rm SM}(q^2+m_V^2)}\right)^2 \times \left[\frac{d\sigma}{dE_{nr}}\right]_{\rm SM}^{\nu N}, \tag{9}$$

where α_{em} is the fine structure constant, while m_μ and m_τ denote the muon and tau masses, respectively,[4] and the plus (minus) sign accounts for ν_μ-nucleus (ν_τ-nucleus) scattering.

III. ELASTIC NEUTRINO-ELECTRON SCATTERING

Proceeding in an analogous way as in the case of CEνNS, in this section we discuss the formalism describing EνES within and beyond the SM.

A. EνES through SM interaction channel

EνES is a well-understood weak flavored process where (anti)neutrinos of flavor $\alpha = \{e, \mu, \tau\}$ interact with electrons via elastic scattering at low and intermediate energies, receiving contributions from both neutral and charged currents for $\alpha = e$, and neutral current only for $\alpha = \{\mu, \tau\}$. Within the framework of the SM, the Lagrangian density corresponding to the process $\overset{(-)}{\nu}_e + e^- \to \overset{(-)}{\nu}_e + e^-$, reads[5] [65]

$$\begin{aligned}\mathcal{L}_{\rm SM}(\overset{(-)}{\nu}_e + e^- \to \overset{(-)}{\nu}_e + e^-) &= -\frac{G_F}{\sqrt{2}}\{[\bar{\nu}_e\gamma^\rho(1-\gamma_5)e][\bar{e}\gamma_\rho(1-\gamma_5)\nu_e] \\ &\quad + [\bar{\nu}_e\gamma^\rho(1-\gamma_5)\nu_e][\bar{e}\gamma_\rho(g_V - g_A\gamma_5)e]\},\end{aligned} \tag{10}$$

while at the tree level the corresponding differential cross section with respect to the electron recoil energy E_{er}, is given as [66]

$$\left[\frac{d\sigma_{\nu_\alpha}}{dE_{er}}\right]_{\rm SM}^{\nu e} = \frac{G_F^2 m_e}{2\pi}\left[(g_V+g_A)^2 + (g_V-g_A)^2\left(1-\frac{E_{er}}{E_\nu}\right)^2 - (g_V^2 - g_A^2)\frac{m_e E_{er}}{E_\nu^2}\right]. \tag{11}$$

In Eq. (11), g_V and g_A are vector and axial vector couplings, respectively, and take the form

[3] In Ref. [16] the P contribution to CEνNS was reported to be vanishing based on the fact that the corresponding nucleon matrix element is vanishing [59,60].

[4] For a study focusing on models with an extra $U_{B-2L_\alpha-L_\beta}$ and U_{B-3L_α} gauge symmetry, see Ref. [64].

[5] For the case of $\nu_{\mu,\tau}$–e^- EνES, the Lagrangian involves only neutral-current terms.

$$g_V = -\frac{1}{2} + 2\sin^2\theta_W + \delta_{\alpha e}, \qquad g_A = -\frac{1}{2} + \delta_{\alpha e}, \tag{12}$$

where the $\delta_{\alpha e}$ term is the Kronecker delta, which becomes nonzero only for ν_e–e^- interactions. For the case of antineutrino scattering, the EνES cross section is given by Eq. (11) with the substitution $g_A \to -g_A$.

B. EνES through light novel mediators

Similar to the CEνNS case, here also we consider all possible EνES contributions arising from the Lorentz-invariant forms $X = \{S, P, V, A, T\}$. For light vector and axial vector novel mediators, the total differential cross sections can be achieved by replacing g_V and g_A from the SM cross section as [67,68]

$$g'_{V/A} = g_{V/A} + \frac{g_{\nu V/A} \cdot g_{eV/A}}{4\sqrt{2}G_F(2m_e E_{er} + m^2_{V/A})}. \tag{13}$$

It is interesting to notice that in the U_{B-L} gauge extension the cross section is also given by Eq. (13) since $Q'_\ell = Q'_\nu = -1$, while in the universal case it holds that $Q'_\ell = Q'_\nu = 1$, hence both cases leading to $g_{\nu V/A} = g_{eV/A}$ in Eq. (13). On the other hand, under $U_{L_\mu - L_\tau}$ symmetry, the new light vector mediator contributes at one-loop level for $\sigma_{\nu_\mu - e}$ and $\sigma_{\nu_\tau - e}$ only, while $\sigma_{\nu_e - e}$ is vanishing.[6] The relevant couplings read [62]

$$g'_V = g_V \pm \frac{\alpha_{em}}{3\sqrt{2}\pi G_F}\log\left(\frac{m^2_\tau}{m^2_\mu}\right)\frac{g_{\nu V} \cdot g_{\mathrm{eV}}}{(2m_e E_{er} + m^2_V)}, \tag{14}$$

where, unlike the CEνNS case, the plus (minus) sign corresponds to $\sigma_{\nu_\tau - e}$ ($\sigma_{\nu_\mu - e}$) scattering. The remaining S, P, and T cross section contributions add incoherently to the SM cross section and have been previously written as [10,69]

$$\left[\frac{d\sigma_{\nu_\alpha}}{dE_{er}}\right]^{\nu e}_S = \left[\frac{g^2_{\nu S} \cdot g^2_{eS}}{4\pi(2m_e E_{er} + m^2_S)^2}\right]\frac{m^2_e E_{er}}{E^2_\nu}, \tag{15}$$

$$\left[\frac{d\sigma_{\nu_\alpha}}{dE_{er}}\right]^{\nu e}_P = \left[\frac{g^2_{\nu P} \cdot g^2_{eP}}{8\pi(2m_e E_{er} + m^2_P)^2}\right]\frac{m_e E^2_{er}}{E^2_\nu}, \tag{16}$$

$$\left[\frac{d\sigma_{\nu_\alpha}}{dE_{er}}\right]^{\nu e}_T = \frac{m_e \cdot g^2_{\nu T} \cdot g^2_{eT}}{2\pi(2m_e E_{er} + m^2_T)^2} \cdot \left[1 + 2\left(1 - \frac{E_{er}}{E_\nu}\right) + \left(1 - \frac{E_{er}}{E_\nu}\right)^2 - \frac{m_e E_{er}}{E^2_\nu}\right]. \tag{17}$$

[6]Nonzero couplings contribute to $\sigma_{\nu_e - e}$ at two-loop level through $Z_0 - V$ mixing, which are neglected in this work.

TABLE II. Neutrino end point energy and flux normalization for the different astrophysical neutrino sources. The flux normalizations are taken from Ref. [76].

Component	$E_\nu^{\max}$ (MeV)	Flux (cm^{-2} s^{-1})
pp	0.42341	5.98×10^{10}
pep	1.44	1.44×10^{8}
$^7\mathrm{Be}_{\mathrm{High}}$	0.8613	4.35×10^{9}
$^7\mathrm{Be}_{\mathrm{Low}}$	0.3843	4.84×10^{8}
^{8}B	16.36	5.25×10^{6}
hep	18.784	7.98×10^{3}
^{13}N	1.199	2.78×10^{8}
^{15}O	1.732	2.05×10^{8}
^{17}F	1.74	5.29×10^{6}
Atm.	981.75	10.5
DSN	91.201	86

IV. RESULTS

A. CEνNS and EνES events at direct detection dark matter detectors

In our analysis, we consider astrophysical neutrinos coming from the Sun [70], the atmosphere [71], and diffuse supernovae (DSN) [72]. In our calculations, we have neglected the neutrino contributions coming from Earth, known as geoneutrinos, as their induced events are expected to be overshadowed by several orders of magnitude with respect to solar neutrinos [73–75]. For the normalization of the different neutrino fluxes, we use the recommended conventions reported in Ref. [76], which are listed in Table II.

For the interaction channel X, the differential event rate of CEνNS at a given detector follows from the convolution of the differential cross section with the neutrino energy distribution $d\Phi/dE_\nu$, as[7] [48]

$$\left[\frac{dR}{dE_{nr}}\right]^{\nu N}_X = t_{\mathrm{run}} N_{\mathrm{target}} \mathcal{A}(E_{nr}) \sum_i \int_{E_\nu^{\min}}^{E_\nu^{\max}} dE_\nu \frac{d\Phi_i(E_\nu)}{dE_\nu} \times \left[\frac{d\sigma}{dE_{nr}}(E_\nu, E_{nr})\right]^{\nu N}_X, \tag{18}$$

where $\mathcal{A}(E_{nr})$ is the detection efficiency, t_{run} denotes the exposure time, and N_{target} represents the number of target nuclei. In the latter expression, the index i runs over all the neutrino sources with energy distribution $d\Phi_i/dE_\nu$ and $E_\nu^{\max}$ denotes the maximum neutrino energy of the ith source (see Table II). Finally, the minimum neutrino energy $E_\nu^{\min}$ required to generate a nuclear recoil with energy E_{nr} is trivially obtained from the kinematics of the process and reads

[7]An ideal detector with perfect efficiency and resolution power is assumed.

$$E_\nu^{\min} = \frac{1}{2}\left[E_{nr} + \sqrt{E_{nr}^2 + 2m_N E_{nr}}\right] \approx \sqrt{\frac{m_N E_{nr}}{2}}. \quad (19)$$

In our analysis, we also consider corrections from detector-specific quantities. In particular, for the ionization xenon detectors considered here, a significant amount of nuclear recoil energy E_{nr} is lost into heat and other dissipative energies, so that the actual energy measured by the detector is an electron equivalent energy E_{er} [77]. In our calculation, this effect is taken into account through the quenching factor $\mathcal{Q}_f(E_{nr})$, calculated on the basis of theoretical predictions within Lindhard theory [78]

$$\frac{E_{er}}{E_{nr}} = \mathcal{Q}_f(E_{nr}) = \frac{kg(\gamma)}{1 + kg(\gamma)}, \quad (20)$$

where $g(\gamma) = 3\gamma^{0.15} + 0.7\gamma^{0.6} + \gamma$, with $\gamma = 11.5 \cdot Z^{-\frac{7}{3}} E_{nr}(\mathrm{keV_{nr}})$ and $k = 0.133 \cdot Z^{\frac{2}{3}} A^{-\frac{1}{2}}$. Let us stress that, for the case of germanium, low-energy corrections to the quenching factor can been accounted for through the adiabatic correction of Lindhard theory, introduced in Ref. [79].[8] After incorporating the quenching factor corrections, the number of events in the jth bin is written as

$$[R_j]_X^{\nu N} = \int_{E_{er}^j}^{E_{er}^{j+1}} dE_{er} \left[\frac{dR}{dE_{nr}}\right]_X^{\nu N} \frac{1}{\mathcal{Q}_f}\left(1 - \frac{E_{er}}{\mathcal{Q}_f}\frac{d\mathcal{Q}_f}{dE_{er}}\right). \quad (21)$$

At this point, we turn our attention to EνES. For the case of solar neutrinos, the differential number of events takes into account the effect of neutrino oscillations in propagation and is given according to the expression [81]

$$\left[\frac{dR}{dE_{er}}\right]_X^{\nu e} = t_{\mathrm{run}} N_{\mathrm{target}} \mathcal{A}(E_{er}) \sum_{i=\mathrm{solar}} \int_{E_\nu^{\min}}^{E_\nu^{\max}} dE_\nu \frac{d\Phi_i^{\nu_e}(E_\nu)}{dE_\nu} \times \left(P_{ee}\left[\frac{d\sigma_{\nu_e}}{dE_{er}}\right]_X^{\nu e} + \overline{P_{ef}}\left[\frac{d\sigma_{\nu_f}}{dE_{er}}\right]_X^{\nu e}\right), \quad (22)$$

with $f = \mu, \tau$ and the minimum neutrino energy being

$$E_\nu^{\min} = \frac{1}{2}\left[E_{er} + \sqrt{E_{er}^2 + 2m_e E_{er}}\right]. \quad (23)$$

Since the EνES cross section is not flavor blind as the CEνNS one, Eq. (22) incorporates neutrino oscillations by weighting the flavored cross section with the corresponding oscillation probability. For our purposes, it is sufficient to consider the averaged oscillation probability $P_{ee}(E_\nu)$ in the two-flavor approximation, which we take from [82]. Notice that in the second term of Eq. (22) the oscillation factors read $\overline{P_{e\mu}} \equiv (1 - P_{ee})\cos^2\theta_{23}$ and $\overline{P_{e\tau}} \equiv (1 - P_{ee})\sin^2\theta_{23}$ for incoming ν_μ and ν_τ neutrinos, respectively.[9] Let us note that, for the case of atmospheric and DSN neutrinos, oscillation effects are neglected. This is a reasonable approximation given the fact that the expected EνES event rates from atmospheric and DSN neutrinos are suppressed by several orders of magnitude compared to the dominant solar ones (see the discussion below). Therefore, in our statistical analysis this approximation is not expected to have any quantitative effect. The differential number of EνES events relevant to atmospheric and DSN neutrinos is then calculated as

$$\left[\frac{dR}{dE_{er}}\right]_X^{\nu e} = t_{\mathrm{run}} N_{\mathrm{target}} \mathcal{A}(E_{er}) \sum_{i=\mathrm{atm,DSN}} \int_{E_\nu^{\min}}^{E_\nu^{\max}} dE_\nu \frac{d\Phi_i^{\nu_\alpha}(E_\nu)}{dE_\nu}\left[\frac{d\sigma_{\nu_\alpha}}{dE_{er}}\right]_X^{\nu e}, \qquad \nu_\alpha = \{\nu_e, \bar{\nu}_e, \nu_{\mu,\tau}, \bar{\nu}_{\mu,\tau}\}. \quad (24)$$

Up to this point, for all EνES interaction channels within and beyond the SM, our discussion applies to the case where neutrinos scatter off free electrons. However, the target electrons are not free, but rather bounded inside the atom. Therefore, in order to perform realistic simulations of the expected number of events at a given detector, atomic binding effects should be also considered. To account for binding effects in our analysis, the free EνES cross section $(d\sigma_{\nu_\alpha}/dE_{er})_{\mathrm{free}}$ defined in Eqs. (11)–(17) is weighted by a series of step functions introduced in Ref. [84] as follows:

$$\left[\frac{d\sigma_{\nu_\alpha}}{dE_{er}}\right]_X^{\nu e} = \frac{1}{Z}\sum_{i=1}^{Z} \Theta(E_{er} - B_i)\left(\left[\frac{d\sigma_{\nu_\alpha}}{dE_{er}}\right]_X^{\nu e}\right)_{\mathrm{free}}. \quad (25)$$

Here, $\Theta(x)$ is the Heaviside step function, while the quantity $\sum_{i=1}^{Z}\Theta(E_{er} - B_i)$ quantifies the number of electrons that can be ionized by the recoil energy E_{er}, and B_i represents the binding energy of the ith electron in the atom. The single-particle atomic level binding energy of electrons in a ^{131}Xe atom is given in Table III [84].

[8] Because of the lack of data for the xenon isotope we are interested in this work, we have verified that our results remain unaffected even when considering $\pm 1\sigma$ deviations from the adiabatic parameter corresponding to germanium (see Table I of Ref. [79]). Improved quenching factors at sub-keV energies are comprehensively discussed in Ref. [80].

[9] The value of the atmospheric mixing angle (θ_{23}) is taken from the best fit of the 2020 Valencia global fit [83].

Assuming typical benchmark values $g_X^2 = 10^{-4}$ and $m_X = 1$ GeV, differential and integrated CEνNS (EνES) event rates above threshold for a xenon target (assuming average isotopic abundance) are shown in the left (right) panel of Fig. 1 as functions of the recoil energy for all possible interactions X. It is interesting to notice that, in general, the CEνNS number of events are expected to exceed the EνES rate by several orders of magnitude. However, for a realistic next generation experiment operating with typical threshold energies, i.e., $E_{er} > 0.1$ keV$_{ee}$, this is not strictly true. First, for $E_{er} > 0.1$ keV$_{ee}$ it becomes evident that CEνNS-induced events will be dominated by ^{8}B neutrinos, while the EνES ones will be dominated by pp neutrinos. Then, from a closer inspection of the graphs it can be deduced that CEνNS and EνES are expected to generate a comparable number of events (at least) within the SM. This can be understood as follows. Although the CEνNS cross section scales with

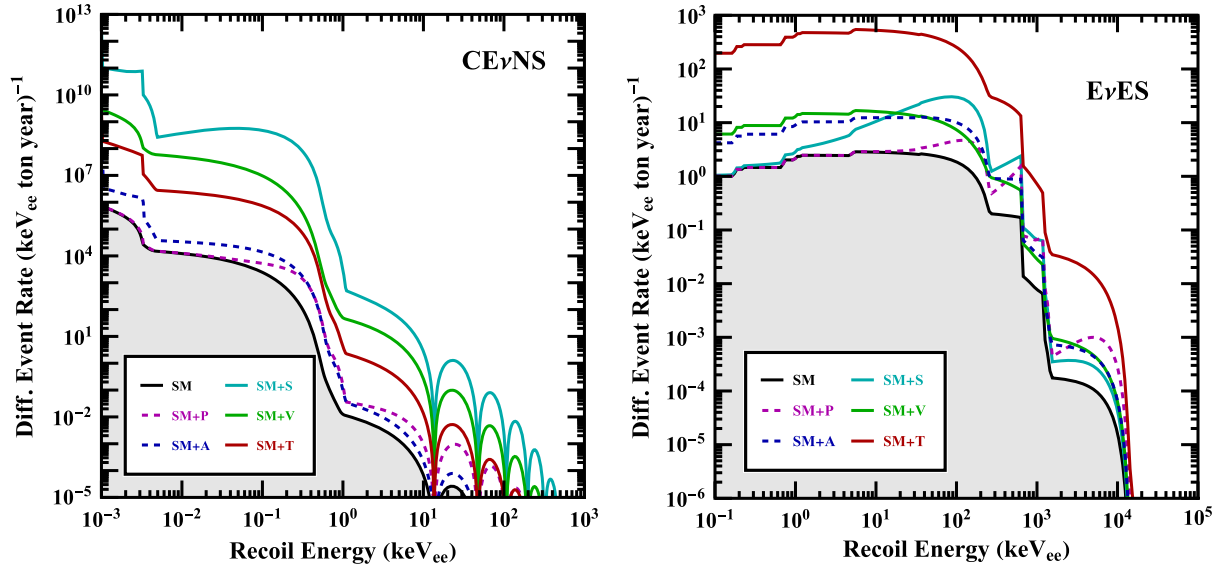

(a) Differential event spectra for CEνNS (left) and EνES (right) processes.

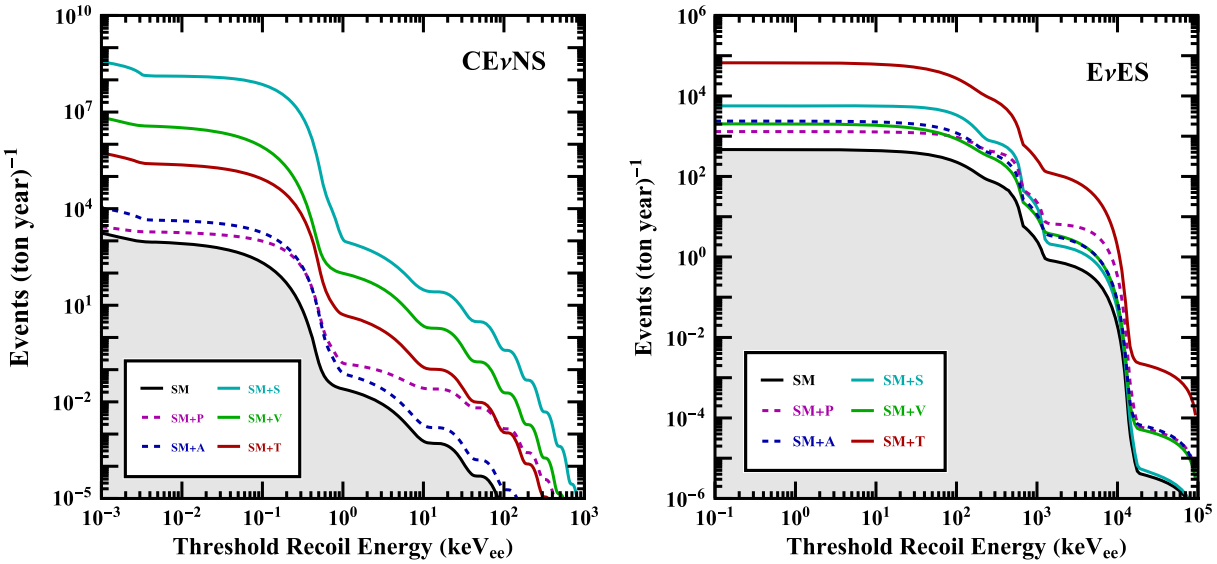

(b) Integrated event spectra for CEνNS (left) and EνES (right) processes.

FIG. 1. Differential (a) and integrated (b) event spectra expected at a xenon target for CEνNS and EνES processes as a function of the recoil energy (threshold recoil energy) measured in keV$_{ee}$ units. The contributions from the different new physics interactions X are calculated assuming the benchmark values $g_X^2 = 10^{-4}$ and $m_X = 1$ GeV (for details, see the text).

TABLE III. Single-particle (SP) energies for the xenon atom derived from Hartree-Fock calculations in Ref. [84].

State	SP (eV)	State	SP (eV)	State	SP (eV)	State	SP (eV)
$^1s_{\frac{1}{2}}$	34759.3	$^3p_{\frac{3}{2}}$	1024.8	$^4p_{\frac{3}{2}}$	708.1	$^5p_{\frac{1}{2}}$	13.4
$^2s_{\frac{1}{2}}$	5509.8	$^3p_{\frac{1}{2}}$	961.2	$^4p_{\frac{1}{2}}$	162.8	$^5p_{\frac{3}{2}}$	12.0
$^2p_{\frac{3}{2}}$	5161.5	$^3d_{\frac{5}{2}}$	708.1	$^4d_{\frac{5}{2}}$	73.8		
$^2p_{\frac{1}{2}}$	4835.6	$^3d_{\frac{3}{2}}$	694.9	$^4d_{\frac{3}{2}}$	71.7		
$^3s_{\frac{1}{2}}$	1170.5	$^4s_{\frac{1}{2}}$	229.4	$^5s_{\frac{1}{2}}$	27.5		

$\sim N^2$ as a consequence of the coherency in neutrino-nucleus scattering, the EνES-induced number of events is enhanced by an overall multiplicative factor Z coming due to the number of electron targets, while the remaining difference, which is of the order of an overall factor $\sim N$, is compensated by the relative difference of ^{8}B and pp flux normalization. Before closing this discussion, let us note the impact of nuclear (atomic) effects in the CEνNS (EνES) rates. In particular, as can be seen from the CEνNS spectral rates, the various dips occurring for $E_{er} > 25$ keV$_{\rm ee}$ are due to the minima of the nuclear form factor (see Fig. 3 of Ref. [85]), while the slight suppression of the EνES rates occurring for recoil energies below $\sim$35 keV$_{\rm ee}$ reflects the atomic binding effects (see Table III).

B. Sensitivity on S, P, V, A, T interactions

At this point, we are interested to explore the projected sensitivities on the $(m_X,\ g_X)$ parameter space at a typical next generation experiment looking for direct detection of dark matter. For estimating the projected sensitivities of the next generation experiments to the various new interaction channels $X = \{S, P, V, A, T\}$, we perform a spectral fit in terms of the χ^2 function [86]

$$\chi^2(\xi, m_X, g_X) = 2\sum_{i=1}^{n_{\rm bins}}\left[R^i_{\rm pred}(\xi, m_X, g_X) - R^i_{\rm exp} + R^i_{\rm exp}\ln\left(\frac{R^i_{\rm exp}}{R^i_{\rm pred}(\xi, m_X, g_X)}\right)\right] + \left(\frac{\xi}{\sigma_{\rm sys}}\right)^2, \tag{26}$$

where ξ denotes a nuisance parameter to account for the various systematic uncertainties. The expected number of events in the ith bin is defined as $R^i_{\rm exp} = R^i_{\rm SM} + R^i_{\rm bg}$, with $R^i_{\rm bg}$ being the number of background events, while the predicted number of events in the presence of the interaction X is $R^i_{\rm pred} = (1+\xi)[R^i_{X+{\rm SM}}(m_X, g_X) + R^i_{\rm bg}]$. At this point, we should stress that, in our EνES-based statistical analysis, the atmospheric and DSN fluxes are safely neglected. Indeed, this is a reasonable approximation given the expected SM event rates depicted in the right panel of Fig. 1. In the present work, we will consider two representative case studies accounting for different detector-specific quantities, namely, an "optimistic" and a "realistic" scenario. The two scenarios differ in the details of the detector properties and effects that are taken into account. One of our aims is to compare and contrast the results obtained from an ideal vs realistic detector. The details of the two scenarios are as described below.

(i) Optimistic scenario: A xenon detector with a 1 ton · yr exposure is assumed. This is, however, a conservative choice that exceeds slightly the 0.65 ton · yr achieved by XENON1T [87] and by a factor 20 less than the exposure goal of 20 ton · yr at XENONnT [44]. We stick to the latter choice to avoid potential overestimation of our projected sensitivities, since for this scenario the detector efficiency and energy resolution are not taken into consideration. For both CEνNS and EνES analyses, we consider a flat background taken to be 10% of the SM events, as well as a systematic uncertainty $\sigma_{\rm sys} = 10\%$. For our spectral fit we consider 100 log-spaced bins in the range $(0.1, 100)$ keV$_{\rm ee}$ for the case of CEνNS and in the range $(0.1, 10^4)$ keV$_{\rm ee}$ for the case of EνES. Let us clarify that our optimistic scenario assumes a threshold as low as 0.1 keV$_{\rm ee}$ and a perfect efficiency, which is motivated by the "$S2$-only" analysis done in Ref. [88]. For the case of EνES we have also checked that our projected sensitivities remain the same if a narrower recoil window $(0.1, 100)$ keV$_{\rm ee}$ is chosen.

(ii) Realistic scenario: This scenario will also serve as reference point to highlight and contrast the results expected from an ideal and a realistic detector. We consider the planned 20 ton · yr exposure foreseen at XENONnT, and we incorporate realistic backgrounds, efficiency, and resolution effects. In particular, for our CEνNS analysis we consider the neutron background[10] from Ref. [44] and the efficiency from Ref. [89]. For our EνES analysis, the background model B_0 (appropriately scaled to account for the 20 ton · yr exposure) and the detection efficiency, are both taken from Ref. [87]. Moreover, our theoretical EνES event rates are eventually smeared[11] by taking into account the energy resolution power of XENON1T, that is, $\sigma(E) = a\cdot\sqrt{E} + b\cdot E$, with E being the

[10]For this particular case, due to lack of information we do not assign any uncertainty on the neutron background, i.e., our predicted number of events in this case reads $R^i_{\rm pred} = (1+\xi)[R^i_{X+{\rm SM}}(m_X, g_X)] + R^i_{\rm bg}$. We have checked, however, that our result remains essentially unaltered if a background uncertainty as high as 10% is assumed.

[11]This requires another integration of Eq. (22) over the true recoil energy E_{er} taking the resolution function to be a normalized Gaussian, see Ref. [90].

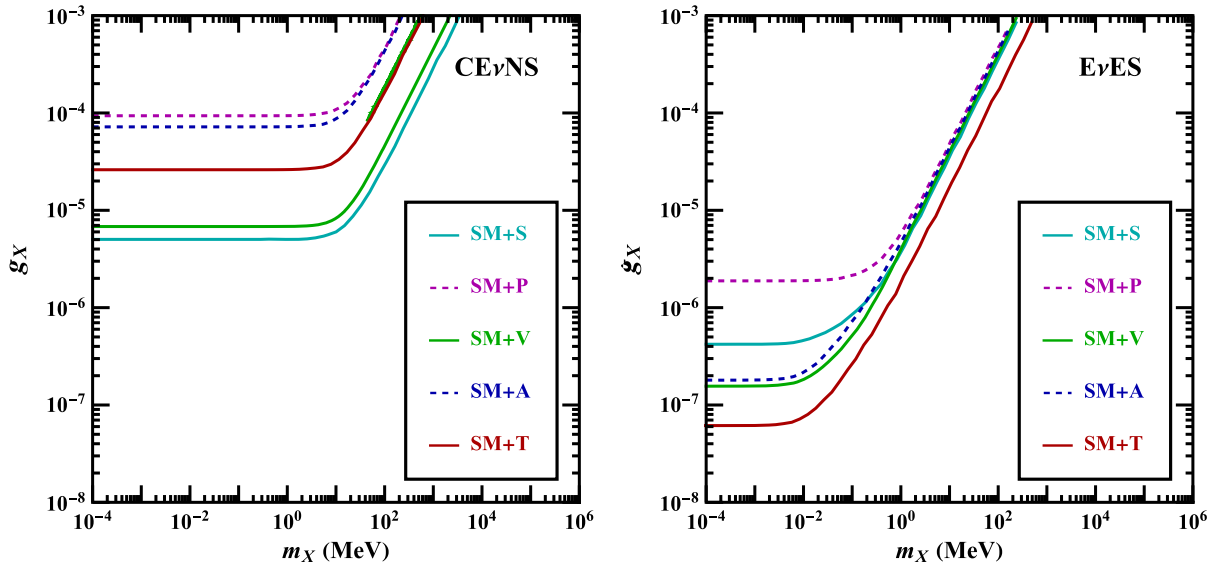

(a) **Optimistic scenario**

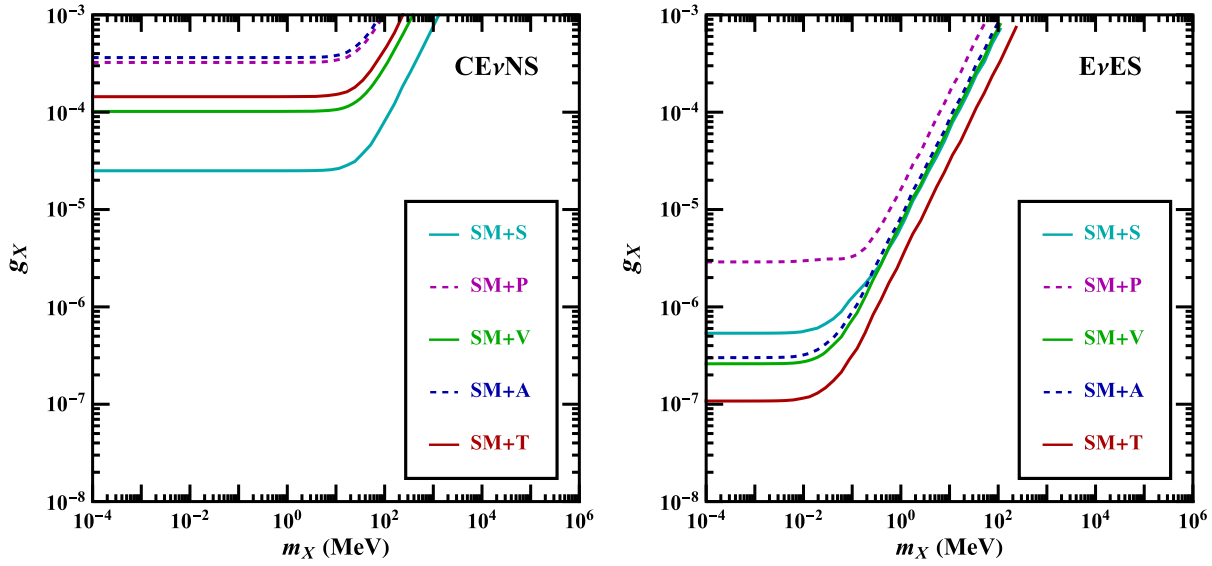

(b) **Realistic scenario**

FIG. 2. Projected sensitivities for the various $X = \{S, P, V, A, T\}$ interactions for CEνNS (left) and EνES (right). The results are presented at 90% C.L. Graphs correspond to the (a) optimistic and (b) realistic scenarios.

reconstructed recoil energy, $a = 0.310\ \sqrt{\text{keV}_{\text{ee}}}$, and $b = 0.0037\ \text{keV}_{\text{ee}}$ [87]. We consider 17 linearly spaced bins in the range $(4, 52)\ \text{keV}_{\text{nr}}$ for our CEνNS analysis and 30 linearly spaced bins in the range $(0, 30)\ \text{keV}_{\text{ee}}$ for our EνES analysis [44]. Finally, a 10% systematic uncertainty is assigned for CEνNS as in the optimistic scenario, while for the case of EνES a 3% systematic uncertainty is taken to account for the detection uncertainty of XENON1T.

The resulting projected sensitivities in the $(m_X,\ g_X)$ parameter space are illustrated at 90% C.L. in the left and right panels of Fig. 2, respectively, while upper (lower) panels correspond to the optimistic (realistic) scenario. As can be seen, in a future CEνNS (EνES) measurement among the different interaction channels the scalar (tensor) interaction will be constrained with maximum sensitivity, while for both CEνNS and EνES the pseudoscalar interaction will be the least constrained. A direct comparison of CEνNS and EνES sensitivities leads to the conclusion that

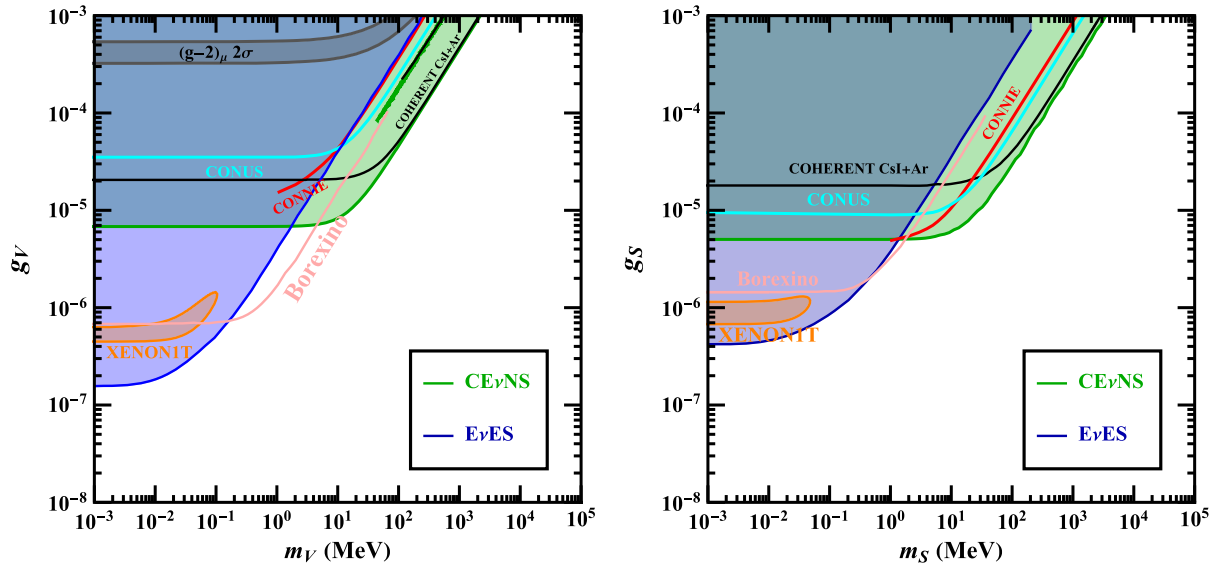

(a) **Optimistic scenario:** For the universal vector (left) and the scalar (right) mediators.

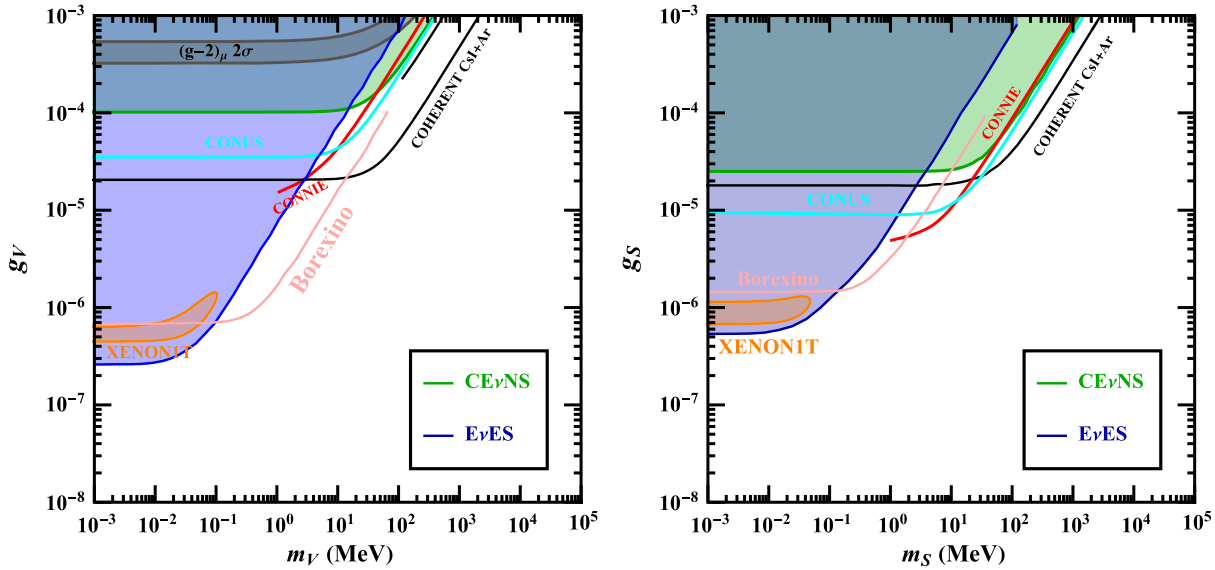

(b) **Realistic scenario:** For the universal vector (left) and the scalar (right) mediators.

FIG. 3. Projected sensitivity at 90% C.L. in the parameter space (m_V, g_V) for the universal vector mediator model (left) and in (m_S, g_S) for a scalar mediator model (right). Graphs correspond to the (a) optimistic and (b) realistic scenarios. A comparison is given with existing constraints from dedicated CEνNS experiments and XENON1T (see the text).

future EνES measurements will be a more powerful probe for the investigation of novel light mediators.

At this point it is interesting to compare our projected sensitivities with existing constraints in the literature. First, by focusing on the universal light vector mediator scenario, in the left panel of Fig. 3 we compare our present results at 90% C.L. with existing constraints from the combined analysis of COHERENT CsI + Ar data [63], the recent CONNIE [29] and CONUS [30] data, and the Borexino analysis of Ref. [91], as well as the anomalous magnetic moment of the muon reported in Ref. [4]. Also shown are the corresponding 90% C.L. constraints coming from the XENON1T excess using EνES calculated in this work. Our optimistic scenario coincides with the XENON1T setup, hence the improvement on our EνES-based constraints is driven by the factor ~20 larger exposure considered in the present analysis, while the shape difference is due to the XENON1T excess data (SM expectation) considered as

$R_{\rm exp}$ for the XENON1T (optimistic scenario) analysis. The Borexino limits of Ref. [91] extend to larger mediator masses compared to our present results, since the analysis has been performed considering a larger recoil energy window, covering also CNO and ^{8}B neutrinos. By comparing the upper and lower graphs, we conclude that constraints from dedicated CEνNS experiments will be overridden by the future CEνNS measurements at direct detection dark matter detectors, given that the threshold and detection efficiencies will improve and the backgrounds will become even better understood. Finally, it becomes evident that the EνES channel dominates over CEνNS in the low mass region for $m_V \leq 2$ MeV.

Similar conclusions are drawn for the case of a scalar mediator, as shown in the right panel of Fig. 3. Available results can be found from CEνNS analyses in Refs. [29,30,63] and from the interpretation of XENON1T excess performed in this work (see also Refs. [8,9]). Regarding the cases of S, V, A interactions for both CEνNS and EνES channels, as well as for the case of P using EνES only, results corresponding to the optimistic case can be found in Ref. [16]. Let us note, however, that in the latter work the sensitivities were obtained by assuming different experimental configurations, as well as by neglecting quenching and atomic effects for CEνNS and EνES, respectively. Regarding the cases of P and T interactions, preliminary results have been presented in Ref. [54] by analyzing the COHERENT data. Again, the future sensitivities discussed here are about 1 order of magnitude more stringent than other studies. Finally, to the best of our knowledge, studies corresponding to our realistic case have not been done for any kind of model-dependent or -independent light mediator.

We finally turn our attention to the vector mediator interactions predicted within the U_{B-L} and $U_{L_\mu - L_\tau}$ gauge extensions. Before proceeding with the discussion of our statistical analysis, let us provide some clarifications regarding the calculation of the number of CEνNS and EνES events within the $L_\mu - L_\tau$ model. Since the $\nu_e - e^-$ coupling is vanishing, we neglect the first term in Eq. (22) and therefore a large portion of the solar neutrino flux will not contribute to the expected EνES rates. Likewise, in our CEνNS-based analysis we consider only the oscillated $\nu_{\mu,\tau}$ fluxes of solar neutrinos, while from the atmospheric neutrino flux we consider only the relevant ν_μ and $\bar{\nu}_\mu$ components. For atmospheric neutrinos with sub-GeV neutrinos, matter-oscillation effects are negligible [92]. Following the procedure of Ref. [81], one sees that the oscillated fluxes reaching the detector are $\Phi^{\nu_e}_{\rm atm} \approx \tilde{\Phi}^{\nu_e}_{\rm atm}$, $\Phi^{\nu_\mu}_{\rm atm} \approx 2/3\tilde{\Phi}^{\nu_\mu}_{\rm atm}$, and $\Phi^{\nu_\tau}_{\rm atm} \approx 1/3\tilde{\Phi}^{\nu_\mu}_{\rm atm}$, where $\tilde{\Phi}^{\nu_\alpha}_{\rm atm}$ denotes the unoscillated flux reported in Ref. [71]. We have verified that our results remain unaffected when atmospheric neutrino oscillations are explicitly taken into account. Finally, regarding the DSN neutrino flux we assume that roughly $\Phi^{\nu_\mu+\bar{\nu}_\mu}_{\rm DSN} \approx \Phi^{\nu_\tau+\bar{\nu}_\tau}_{\rm DSN}$.

Left and right panels of Fig. 4 illustrate the projected sensitivity at 90% C.L. for the studied $B-L$ and $L_\mu - L_\tau$ model, respectively. The results are shown for both CEνNS and EνES at a future dark matter direct detection experiment with the same general conclusions as discussed previously. Moreover, as expected, the exclusion curves corresponding to the $B-L$ model are more stringent. In order to compare with other experimental probes, existing limits placed by dielectron resonances at ATLAS [93] and electron beam dump fixed target experiments [94,95], as well as dark photon searches at *BABAR* [96,97], KLOE [98], CMS [99], and LHCb [100],[12] are superimposed. Further constraints from the EνES experiments TEXONO, GEMMA, BOREXINO, LSND, and CHARM II can be found in Ref. [101]. Also shown are constraints derived from the analysis of the COHERENT data [63] and the XENON1T excess [9]. For the $L_\mu - L_\tau$ case, limits are available from recent analyses of Borexino data [32,102] and from 4μ searches at *BABAR* [103], CMS [104], and ATLAS [105,106], as well as recasted limits from LHCb [100]. We furthermore show the corresponding sensitivity from the analysis of XENON1T excess performed in this work, by following the procedure of Ref. [8]. As can be seen, our projected sensitivities for CEνNS dominate in mass range $0.1 \leq m_V \leq 1$ GeV, being complementary to *BABAR* and fixed target experiments. In the same vein, our projected sensitivities obtained using EνES are complementary to fixed target experiments and particularly relevant for $m_V \leq 1$ MeV.

Before closing, we should stress that astrophysics and cosmology might place severe bounds to scalar and vector interactions [23]. Those follow mostly from cosmological limits on the sum of neutrino masses, Supernova/stellar-cooling arguments, and sterile neutrino trapping as detailed in Refs. [9,26] (see also Ref. [107]). Given the large astrophysical uncertainties, such constraints should be considered as order of magnitude estimations, while possible mechanisms to evade them are explained in Ref. [26]. Finally, it should be noted that upcoming experiments also have the potential to probe light mediator particles. However, our results provide about an order of magnitude more constrained bounds than those predicted for other future experiments, such as neutrino trident interactions at DUNE [62], model-dependent constraints for DARWIN [33], and constraints extracted from missing energy searches at NA64μ [33] (for expected limits from future beam dump experiments, such as SHiP and FASER2, see Ref. [107]).

[12] *BABAR*, KLOE, CMS, and LHCb limits, recasted to the $B-L$ case, are obtained using the DARKCAST software package.

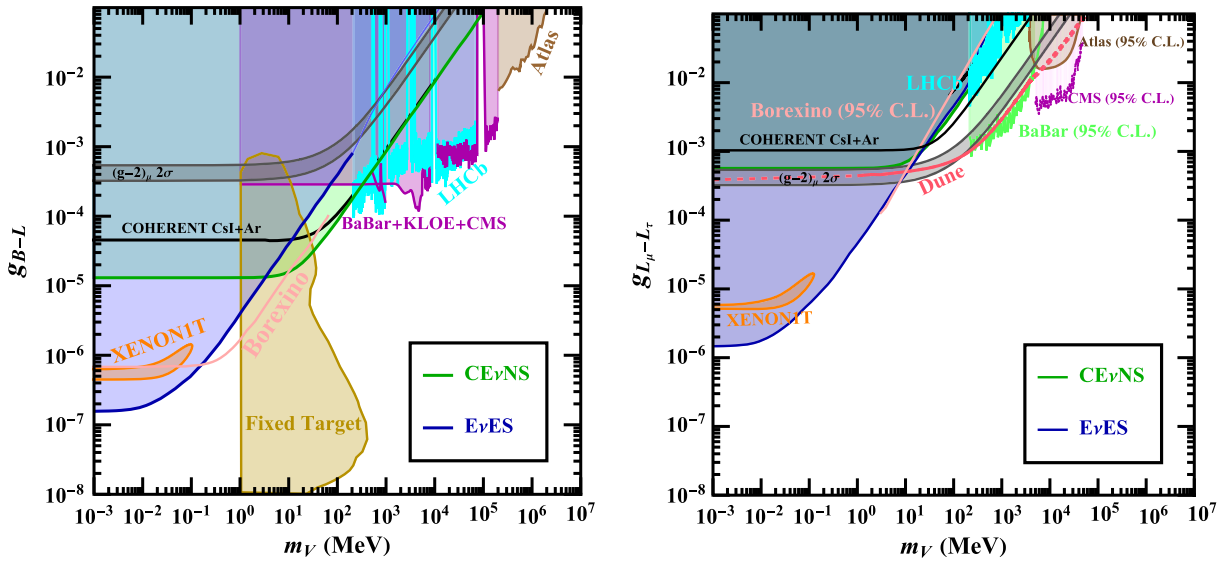

(a) **Optimistic scenario:** For the $B-L$ (left) and $L_\mu - L_\tau$ (right) models.

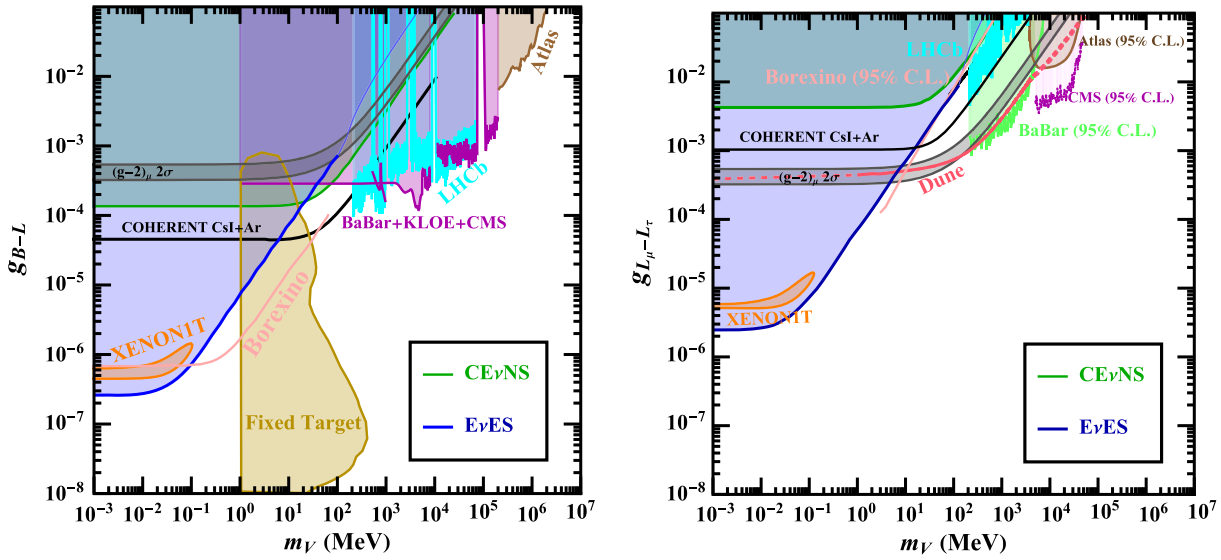

(b) **Realistic scenario:** For the $B-L$ (left) and $L_\mu - L_\tau$ (right) models.

FIG. 4. Projected exclusion curves at 90% C.L. obtained in the present work using CEνNS and EνES for the $B-L$ (left) and $L_\mu - L_\tau$ (right) model. Graphs correspond to the (a) optimistic and (b) realistic scenarios. A comparison with relevant experimental constraints is also given (see the text).

V. CONCLUSIONS

The new era of direct dark matter experiments with multiton mass scale and sub-keV operation threshold makes them favorable facilities with promising prospects for detecting astrophysical neutrino backgrounds to dark matter. Prompted by the latter, we estimated the projected sensitivities to general Lorentz-invariant $X = \{S, P, V, A, T\}$ interactions through CEνNS- and EνES-induced signals. With respect to light vector mediators, our study also considered the case of well-known U_{B-L} and $U_{L_\mu - L_\tau}$ anomaly-free models. To maximize the reliability of event rate simulations, important corrections from detector-specific quantities were taken into account, such as the quenching factor and atomic binding effects for the case of CEνNS and EνES, respectively. Our statistical analysis was performed under the assumption of two benchmark scenarios, which allowed us to compare the maximum potential of a future direct dark matter detection experiment with the expected sensitivities when current detector specifications are explicitly accounted for.

In the optimistic scenario, we assumed a rather low detection threshold of 0.1 $\mathrm{keV_{ee}}$, which would correspond to an ionization-only analysis with a 100% detection efficiency. In our goal to make our analysis as quantitative as possible, in the realistic scenario the effects of finite detection efficiency, nonflat backgrounds, and energy resolutions have been incorporated. We furthermore considered an exposure between 1 and 20 ton · yr, which is readily achievable by the current and future xenon detector technologies. Our present results imply that future CEνNS or EνES measurements at a direct detection dark matter experiment will not only become sensitive to neutrinos coming (mainly) from the Sun, but will also offer competitive constraints to existing ones from dedicated CEνNS and EνES experiments, if backgrounds are under control and sub-keV thresholds become possible. We have furthermore illustrated that the expected sensitivities will cover a large part of the parameter space, previously unexplored from collider probes and beam dump experiments, improving upon the existing bounds by about 1 order of magnitude.

ACKNOWLEDGMENTS

The authors are indebted to D. Aristizabal-Sierra for carefully reading the manuscript and for insightful comments. The authors also acknowledge P. Martínez-Miravé, M. Williams, P. Ilten, K. Ni, F. Gao, and J. Pienaar for useful correspondence. The research of D. K. P. is cofinanced by Greece and the European Union (European Social Fund—ESF) through the operational program "Human Resources Development, Education, and Lifelong Learning" in the context of the project "Reinforcement of Postdoctoral Researchers—2nd Cycle" (MIS-5033021), implemented by the State Scholarships Foundation (IKY). The work of R. S. is supported by the SERB, Government of India Grant No. SRG/2020/002303.

[1] P. Langacker, The physics of heavy Z' gauge bosons, Rev. Mod. Phys. **81**, 1199 (2009).
[2] M. Dittmar, A.-S. Nicollerat, and A. Djouadi, Z-prime studies at the LHC: An update, Phys. Lett. B **583**, 111 (2004).
[3] B. Abi *et al.* (Muon $g-2$ Collaboration), Measurement of the Positive Muon Anomalous Magnetic Moment to 0.46 ppm, Phys. Rev. Lett. **126**, 141801 (2021).
[4] T. Aoyama *et al.*, The anomalous magnetic moment of the muon in the Standard Model, Phys. Rep. **887**, 1 (2020).
[5] F. Jegerlehner and A. Nyffeler, The muon $g-2$, Phys. Rep. **477**, 1 (2009).
[6] P. Agrawal *et al.*, Feebly-interacting particles: FIPs 2020 workshop report, Eur. Phys. J. C **81**, 1015 (2021).
[7] M. Fabbrichesi, E. Gabrielli, and G. Lanfranchi, *The Dark Photon*, Springer Briefs in Physics (Springer Cham, 2020), https://link.springer.com/book/10.1007/978-3-030-62519-1.
[8] C. Boehm, D. G. Cerdeno, M. Fairbairn, P. A. Machado, and A. C. Vincent, Light new physics in XENON1T, Phys. Rev. D **102**, 115013 (2020).
[9] D. Aristizabal Sierra, V. De Romeri, L. J. Flores, and D. K. Papoulias, Light vector mediators facing XENON1T data, Phys. Lett. B **809**, 135681 (2020).
[10] A. N. Khan, Can nonstandard neutrino interactions explain the XENON1T spectral excess?, Phys. Lett. B **809**, 135782 (2020).
[11] R. D. Peccei and H. R. Quinn, *CP* Conservation in the Presence of Instantons, Phys. Rev. Lett. **38**, 1440 (1977).
[12] S. Weinberg, A New Light Boson?, Phys. Rev. Lett. **40**, 223 (1978).
[13] F. Wilczek, Problem of Strong P and T Invariance in the Presence of Instantons, Phys. Rev. Lett. **40**, 279 (1978).
[14] J. Schechter and J. W. F. Valle, Neutrino decay and spontaneous violation of lepton number, Phys. Rev. D **25**, 774 (1982).
[15] C. Bonilla, S. Centelles-Chuliá, R. Cepedello, E. Peinado, and R. Srivastava, Dark matter stability and Dirac neutrinos using only Standard Model symmetries, Phys. Rev. D **101**, 033011 (2020).
[16] D. G. Cerdeño, M. Fairbairn, T. Jubb, P. A. N. Machado, A. C. Vincent, and C. Bœhm, Physics from solar neutrinos in dark matter direct detection experiments, J. High Energy Phys. 05 (2016) 118; 09 (2016) 048(E).
[17] E. Bertuzzo, F. F. Deppisch, S. Kulkarni, Y. F. Perez Gonzalez, and R. Zukanovich Funchal, Dark matter and exotic neutrino interactions in direct detection searches, J. High Energy Phys. 04 (2017) 073.
[18] D. Akimov *et al.* (COHERENT Collaboration), Observation of coherent elastic neutrino-nucleus scattering, Science **357**, 1123 (2017).
[19] D. Akimov *et al.* (COHERENT Collaboration), First Measurement of Coherent Elastic Neutrino-Nucleus Scattering on Argon, Phys. Rev. Lett. **126**, 012002 (2021).
[20] D. Akimov *et al.*, Measurement of the coherent elastic neutrino-nucleus scattering cross section on CsI by COHERENT, arXiv:2110.07730.
[21] J. B. Dent, B. Dutta, S. Liao, J. L. Newstead, L. E. Strigari, and J. W. Walker, Probing light mediators at ultralow threshold energies with coherent elastic neutrino-nucleus scattering, Phys. Rev. D **96**, 095007 (2017).

[22] J. Liao and D. Marfatia, COHERENT constraints on nonstandard neutrino interactions, Phys. Lett. B **775**, 54 (2017).
[23] Y. Farzan, M. Lindner, W. Rodejohann, and X.-J. Xu, Probing neutrino coupling to a light scalar with coherent neutrino scattering, J. High Energy Phys. 05 (2018) 066.
[24] D. K. Papoulias, COHERENT constraints after the COHERENT-2020 quenching factor measurement, Phys. Rev. D **102**, 113004 (2020).
[25] B. Dutta, S. Liao, S. Sinha, and L. E. Strigari, Searching for beyond the Standard Model Physics with COHERENT Energy and Timing Data, Phys. Rev. Lett. **123**, 061801 (2019).
[26] D. Aristizabal Sierra, B. Dutta, S. Liao, and L. E. Strigari, Coherent elastic neutrino-nucleus scattering in multi-ton scale dark matter experiments: Classification of vector and scalar interactions new physics signals, J. High Energy Phys. 12 (2019) 124.
[27] O. Miranda, D. Papoulias, G. Sanchez Garcia, O. Sanders, M. Tórtola, and J. Valle, Implications of the first detection of coherent elastic neutrino-nucleus scattering (CEvNS) with liquid argon, J. High Energy Phys. 05 (2020) 130.
[28] M. Cadeddu, N. Cargioli, F. Dordei, C. Giunti, Y. F. Li, E. Picciau, and Y. Y. Zhang, Constraints on light vector mediators through coherent elastic neutrino nucleus scattering data from COHERENT, J. High Energy Phys. 01 (2021) 116.
[29] A. Aguilar-Arevalo *et al.* (CONNIE Collaboration), Search for light mediators in the low-energy data of the CONNIE reactor neutrino experiment, J. High Energy Phys. 04 (2020) 054.
[30] H. Bonet *et al.* (CONUS Collaboration), Novel constraints on neutrino physics beyond the standard model from the CONUS experiment, J. High Energy Phys. 05 (2022) 085.
[31] S. Sadhukhan and M. P. Singh, Neutrino floor in leptophilic $U(1)$ models: Modification in $U(1)_{L_\mu - L_\tau}$, Phys. Rev. D **103**, 015015 (2021).
[32] D. W. P. d. Amaral, D. G. Cerdeno, P. Foldenauer, and E. Reid, Solar neutrino probes of the muon anomalous magnetic moment in the gauged $\mathrm{U}(1)_{L_\mu - L_\tau}$, J. High Energy Phys. 12 (2020) 155.
[33] D. Amaral, D. Cerdeno, A. Cheek, and P. Foldenauer, Confirming $U(1)_{L_\mu - L_\tau}$ as a solution for $(g-2)_\mu$ with neutrinos, Eur. Phys. J. C **81**, 861 (2021).
[34] D. G. Cerdeño, M. Cermeño, M. Á. Pérez-García, and E. Reid, Medium effects in supernovae constraints on light mediators, Phys. Rev. D **104**, 063013 (2021).
[35] D. Aristizabal Sierra, V. De Romeri, L. Flores, and D. Papoulias, Impact of COHERENT measurements, cross section uncertainties and new interactions on the neutrino floor, J. Cosmol. Astropart. Phys. 01 (2022) 055.
[36] D. Aristizabal Sierra, V. De Romeri, and N. Rojas, COHERENT analysis of neutrino generalized interactions, Phys. Rev. D **98**, 075018 (2018).
[37] A. N. Khan, W. Rodejohann, and X.-J. Xu, Borexino and general neutrino interactions, Phys. Rev. D **101**, 055047 (2020).
[38] F. Escrihuela, L. Flores, O. Miranda, and J. Rendón, Global constraints on neutral-current generalized neutrino interactions, J. High Energy Phys. 07 (2021) 061.
[39] W. Rodejohann, X.-J. Xu, and C. E. Yaguna, Distinguishing between Dirac and Majorana neutrinos in the presence of general interactions, J. High Energy Phys. 05 (2017) 024.
[40] J. Barranco, A. Bolanos, E. Garces, O. Miranda, and T. Rashba, Tensorial NSI and unparticle physics in neutrino scattering, Int. J. Mod. Phys. A **27**, 1250147 (2012).
[41] D. Papoulias and T. Kosmas, Neutrino transition magnetic moments within the non-standard neutrino–nucleus interactions, Phys. Lett. B **747**, 454 (2015).
[42] D. K. Papoulias and T. S. Kosmas, COHERENT constraints to conventional and exotic neutrino physics, Phys. Rev. D **97**, 033003 (2018).
[43] E. Aprile *et al.* (XENON Collaboration), Search for Coherent Elastic Scattering of Solar ^{8}B Neutrinos in the XENON1T Dark Matter Experiment, Phys. Rev. Lett. **126**, 091301 (2021).
[44] E. Aprile *et al.* (XENON Collaboration), Projected WIMP sensitivity of the XENONnT dark matter experiment, J. Cosmol. Astropart. Phys. 11 (2020) 031.
[45] J. Barranco, O. Miranda, and T. Rashba, Probing new physics with coherent neutrino scattering off nuclei, J. High Energy Phys. 12 (2005) 021.
[46] O. Tomalak, P. Machado, V. Pandey, and R. Plestid, Flavor-dependent radiative corrections in coherent elastic neutrino-nucleus scattering, J. High Energy Phys. 02 (2021) 097.
[47] D. Aristizabal Sierra, R. Branada, O. G. Miranda, and G. Sanchez Garcia, Sensitivity of direct detection experiments to neutrino magnetic dipole moments, J. High Energy Phys. 12 (2020) 178.
[48] D. K. Papoulias, R. Sahu, T. S. Kosmas, V. K. B. Kota, and B. Nayak, Novel neutrino-floor and dark matter searches with deformed shell model calculations, Adv. High Energy Phys. **2018**, 6031362 (2018).
[49] D. K. Papoulias and T. S. Kosmas, Standard and nonstandard neutrino-nucleus reactions cross sections and event rates to neutrino detection experiments, Adv. High Energy Phys. **2015**, 763648 (2015).
[50] R. H. Helm, Inelastic and elastic scattering of 187-Mev electrons from selected even-even nuclei, Phys. Rev. **104**, 1466 (1956).
[51] M. Lindner, W. Rodejohann, and X.-J. Xu, Coherent neutrino-nucleus scattering and new neutrino interactions, J. High Energy Phys. 03 (2017) 097.
[52] K. R. Dienes, J. Kumar, B. Thomas, and D. Yaylali, Overcoming velocity suppression in dark-matter direct-detection experiments, Phys. Rev. D **90**, 015012 (2014).
[53] M. Cirelli, E. Del Nobile, and P. Panci, Tools for model-independent bounds in direct dark matter searches, J. Cosmol. Astropart. Phys. 10 (2013) 019.
[54] M. Demirci and M. F. Mustamin, Probing light new mediators on coherent elastic neutrino-nucleus scattering, Andromeda Proceedings, BSM21 (2021), 10.31526/ACP.BSM-2021.31.
[55] D. Aristizabal Sierra, J. Liao, and D. Marfatia, Impact of form factor uncertainties on interpretations of coherent elastic neutrino-nucleus scattering data, J. High Energy Phys. 06 (2019) 141.

[56] Y. Ema, F. Sala, and R. Sato, Neutrino experiments probe hadrophilic light dark matter, SciPost Phys. **10**, 72 (2021).
[57] J. Ellis, K. A. Olive, and C. Savage, Hadronic uncertainties in the elastic scattering of supersymmetric dark matter, Phys. Rev. D **77**, 065026 (2008).
[58] M. Hoferichter, J. Menéndez, and A. Schwenk, Coherent elastic neutrino-nucleus scattering: EFT analysis and nuclear responses, Phys. Rev. D **102**, 074018 (2020).
[59] H.-Y. Cheng, Low-energy interactions of scalar and pseudoscalar Higgs bosons with baryons, Phys. Lett. B **219**, 347 (1989).
[60] H.-Y. Cheng and C.-W. Chiang, Revisiting scalar and pseudoscalar couplings with nucleons, J. High Energy Phys. 07 (2012) 009.
[61] L. Flores, N. Nath, and E. Peinado, Non-standard neutrino interactions in $U(1)'$ model after COHERENT data, J. High Energy Phys. 06 (2020) 045.
[62] W. Altmannshofer, S. Gori, J. Martín-Albo, A. Sousa, and M. Wallbank, Neutrino tridents at DUNE, Phys. Rev. D **100**, 115029 (2019).
[63] M. A. Corona, M. Cadeddu, N. Cargioli, F. Dordei, C. Giunti, Y. F. Li, E. Picciau, C. A. Ternes, and Y. Y. Zhang, Probing light mediators and $(g-2)_\mu$ through detection of coherent elastic neutrino nucleus scattering at COHERENT, J. High Energy Phys. 05 (2022) 109.
[64] L. M. de la Vega, L. Flores, N. Nath, and E. Peinado, Complementarity between dark matter direct searches and CEνNS experiments in $U(1)'$ models, J. High Energy Phys. 09 (2021) 146.
[65] C. Giunti and C. W. Kim, Fundamentals of Neutrino Physics and Astrophysics, 2007.
[66] B. Kayser, E. Fischbach, S. P. Rosen, and H. Spivack, Charged and neutral current interference in $\nu_e e$ scattering, Phys. Rev. D **20**, 87 (1979).
[67] M. Lindner, F. S. Queiroz, W. Rodejohann, and X.-J. Xu, Neutrino-electron scattering: General constraints on Z' and dark photon models, J. High Energy Phys. 05 (2018) 098.
[68] P. Ballett, M. Hostert, S. Pascoli, Y. F. Perez-Gonzalez, Z. Tabrizi, and R. Z. Funchal, Z's in neutrino scattering at DUNE, Phys. Rev. D **100**, 055012 (2019).
[69] J. M. Link and X.-J. Xu, Searching for BSM neutrino interactions in dark matter detectors, J. High Energy Phys. 08 (2019) 004.
[70] W. Haxton, R. Hamish Robertson, and A. M. Serenelli, Solar neutrinos: Status and prospects, Annu. Rev. Astron. Astrophys. **51**, 21 (2013).
[71] G. Battistoni, A. Ferrari, T. Montaruli, and P. Sala, The atmospheric neutrino flux below 100-MeV: The FLUKA results, Astropart. Phys. **23**, 526 (2005).
[72] J. F. Beacom, The diffuse supernova neutrino background, Annu. Rev. Nucl. Part. Sci. **60**, 439 (2010).
[73] J. Monroe and P. Fisher, Neutrino backgrounds to dark matter searches, Phys. Rev. D **76**, 033007 (2007).
[74] G. B. Gelmini, V. Takhistov, and S. J. Witte, Geoneutrinos in large direct detection experiments, Phys. Rev. D **99**, 093009 (2019).
[75] T. Kosmas, V. Kota, D. Papoulias, and R. Sahu, Coherent elastic neutrino-nucleus scattering (CEνNS) event rates for Ge, Zn and Si detector materials, Phys. Rev. C **104**, 064618 (2021).
[76] D. Baxter *et al.*, Recommended conventions for reporting results from direct dark matter searches, Eur. Phys. J. C **81**, 907 (2021).
[77] J. Lewin and P. Smith, Review of mathematics, numerical factors, and corrections for dark matter experiments based on elastic nuclear recoil, Astropart. Phys. **6**, 87 (1996).
[78] J. Lindhard, M. Scharff, and H. Schiott, Range concepts and heavy ion searches, Mat. Fys. Medd. K. Dan. Vidensk. Selsk **33** (1963), https://www.osti.gov/biblio/4153115-range-concepts-heavy-ion-ranges-notes-atomic-collisions-ii.
[79] B. Scholz, A. Chavarria, J. Collar, P. Privitera, and A. Robinson, Measurement of the low-energy quenching factor in germanium using an ^{88}Y/Be photoneutron source, Phys. Rev. D **94**, 122003 (2016).
[80] Y. Sarkis, A. Aguilar-Arevalo, and J. C. D'Olivo, Study of the ionization efficiency for nuclear recoils in pure crystals, Phys. Rev. D **101**, 102001 (2020).
[81] D. Aristizabal Sierra, N. Rojas, and M. Tytgat, Neutrino non-standard interactions and dark matter searches with multi-ton scale detectors, J. High Energy Phys. 03 (2018) 197.
[82] F. Escrihuela, O. Miranda, M. Tortola, and J. Valle, Constraining nonstandard neutrino-quark interactions with solar, reactor and accelerator data, Phys. Rev. D **80**, 105009 (2009).
[83] P. de Salas, D. V. Forero, S. Gariazzo, P. Martínez-Miravé, O. Mena, C. A. Ternes, M. Tórtola, and J. W. F. Valle, 2020 global reassessment of the neutrino oscillation picture, J. High Energy Phys. 02 (2021) 071.
[84] J.-W. Chen, H.-C. Chi, C. P. Liu, and C.-P. Wu, Low-energy electronic recoil in xenon detectors by solar neutrinos, Phys. Lett. B **774**, 656 (2017).
[85] R. Sahu, D. Papoulias, V. Kota, and T. Kosmas, Elastic and inelastic scattering of neutrinos and weakly interacting massive particles on nuclei, Phys. Rev. C **102**, 035501 (2020).
[86] G. J. Feldman and R. D. Cousins, A unified approach to the classical statistical analysis of small signals, Phys. Rev. D **57**, 3873 (1998).
[87] E. Aprile *et al.* (XENON Collaboration), Excess electronic recoil events in XENON1T, Phys. Rev. D **102**, 072004 (2020).
[88] K. Ni, J. Qi, E. Shockley, and Y. Wei, Sensitivity of a liquid xenon detector to neutrino–nucleus coherent scattering and neutrino magnetic moment from reactor neutrinos, Universe **7**, 54 (2021).
[89] E. Aprile *et al.* (XENON Collaboration), Dark Matter Search Results from a One Ton-Year Exposure of XENON1T, Phys. Rev. Lett. **121**, 111302 (2018).
[90] O. G. Miranda, D. K. Papoulias, M. Tórtola, and J. W. F. Valle, XENON1T signal from transition neutrino magnetic moments, Phys. Lett. B **808**, 135685 (2020).
[91] P. Coloma, M. C. Gonzalez-Garcia, M. Maltoni, J. a. P. Pinheiro, and S. Urrea, Constraining new physics with Borexino phase-II spectral data, arXiv:2204.03011.
[92] A. Friedland, C. Lunardini, and M. Maltoni, Atmospheric neutrinos as probes of neutrino-matter interactions, Phys. Rev. D **70**, 111301 (2004).

[93] M. Aaboud *et al.* (ATLAS Collaboration), Search for high-mass new phenomena in the dilepton final state using proton-proton collisions at $\sqrt{s} = 13$ TeV with the ATLAS detector, Phys. Lett. B **761**, 372 (2016).
[94] R. Harnik, J. Kopp, and P. A. Machado, Exploring nu signals in dark matter detectors, J. Cosmol. Astropart. Phys. 07 (2012) 026.
[95] P. Ilten, Y. Soreq, M. Williams, and W. Xue, Serendipity in dark photon searches, J. High Energy Phys. 06 (2018) 004.
[96] J. Lees *et al.* (*BABAR* Collaboration), Search for a Dark Photon in e^+e^- Collisions at *BABAR*, Phys. Rev. Lett. **113**, 201801 (2014).
[97] J. Lees *et al.* (*BABAR* Collaboration), Search for Invisible Decays of a Dark Photon Produced in e^+e^- Collisions at *BABAR*, Phys. Rev. Lett. **119**, 131804 (2017).
[98] A. Anastasi *et al.* (KLOE-2 Collaboration), Combined limit on the production of a light gauge boson decaying into $\mu^+\mu^-$ and $\pi^+\pi^-$, Phys. Lett. B **784**, 336 (2018).
[99] CMS Collaboration, Search for a narrow resonance decaying to a pair of muons in proton-proton collisions at 13 TeV, https://inspirehep.net/literature/1748026.
[100] R. Aaij *et al.* (LHCb Collaboration), Search for $A' \to \mu^+\mu^-$ Decays, Phys. Rev. Lett. **124**, 041801 (2020).
[101] S. Bilmis, I. Turan, T. M. Aliev, M. Deniz, L. Singh, and H. T. Wong, Constraints on dark photon from neutrino-electron scattering experiments, Phys. Rev. D **92**, 033009 (2015).
[102] S. Gninenko and D. Gorbunov, Refining constraints from Borexino measurements on a light Z'-boson coupled to $L\mu - L\tau$ current, Phys. Lett. B **823**, 136739 (2021).
[103] J. P. Lees *et al.* (*BABAR* Collaboration), Search for a muonic dark force at *BABAR*, Phys. Rev. D **94**, 011102 (2016).
[104] A. M. Sirunyan *et al.* (CMS Collaboration), Search for an $L_\mu - L_\tau$ gauge boson using $Z \to 4\mu$ events in proton-proton collisions at $\sqrt{s} = 13$ TeV, Phys. Lett. B **792**, 345 (2019).
[105] W. Altmannshofer, S. Gori, S. Profumo, and F. S. Queiroz, Explaining dark matter and B decay anomalies with an $L_\mu - L_\tau$ model, J. High Energy Phys. 12 (2016) 106.
[106] G. Aad *et al.* (ATLAS Collaboration), Measurements of Four-Lepton Production at the Z Resonance in pp Collisions at $\sqrt{s} = 7$ and 8 TeV with ATLAS, Phys. Rev. Lett. **112**, 231806 (2014).
[107] A. Das, S. Goswami, V. K. N., and T. K. Poddar, Freeze-in sterile neutrino dark matter in a class of $U(1)'$ models with inverse seesaw, arXiv:2104.13986.